

Design and Control of Aerial Modules for Inflight Self-disassembly

David Saldaña¹, Parakh M. Gupta¹, and Vijay Kumar¹

Abstract—Robotic modular systems have the ability to create and break physical links to self-assemble larger custom robots for general tasks. In case of changes in the task or the environment, they can dynamically self-adapt by self-reconfigure during the mission. However, applying those concepts to flying vehicles is still a challenge. In this paper, we present a novel modular design based on a quadrotor platform that uses a lightweight passive mechanism to dock and undock in midair. Using this mechanism and a control strategy, we can divide a rectangular structure into two sub-structures during flight. The undocking action can be sequentially applied to disassemble structures into individual modules. Since self-assembly methods for aerial vehicles have been proposed in the literature, here we focus on the self-disassembly process. We validate our undocking method and self-disassembly algorithm through experiments with actual modules. We highlight that combining our proposed self-disassembly algorithm and existing self-assembly algorithms, aerial modules are able to perform inflight self-reconfiguration.

Index Terms—Cellular and Modular Robots, Aerial Systems: Mechanics and Control, Mechanism Design.

I. INTRODUCTION

MODULAR autonomous systems can offer rapid response in time-critical situations. Agile individual modules can quickly navigate in cluttered environments with obstacles and narrow spaces. Then, they can rendezvous where the task needs to be performed. The modules can join forces and morph to build custom constructions [1] or manipulate objects [2]. Fast-response actions are crucial in urban scenarios. For example in burning buildings constructing temporary structures can support evacuations. Also, in post-disaster environments or large forests, transporting resources and assembling structures can support search and rescue operations.

Joined forces can be stronger than individual efforts. Modular robots can join forces by creating physical links to increase their capabilities [3], [2]. In aerial vehicles, cooperative efforts have been applied to solve problems in object transportation [4], [5], [2], construction [6], [7], and cargo lifting [8], [9].

Manuscript received: February 25, 2019; Revised May 27, 2019; Accepted Jun 16, 2019.

This paper was recommended for publication by Editor Nak Young Chong upon evaluation of the Associate Editor and Reviewers' comments. *We acknowledge Mark R. Cutkosky at Stanford University for the discussion and ideas about attaching mechanisms; and Luis Guerrero-Bonilla at University of Pennsylvania for his feedback on mechanical systems. We gratefully acknowledge the support of DARPA grant HR00111520020, ONR grants N00014-15-1-2115 and N00014-14-1-0510, ARL grant W911NF-08-2-0004, NSF grant IIS-1426840, and NSF grant 1138847.

¹ The authors are with the GRASP Laboratory, University of Pennsylvania, Philadelphia, PA, USA. E-mails {dsaldana, pmg95, kumar}@seas.upenn.edu.

Digital Object Identifier (DOI): see top of this page.



(a) Four docked modules in a 2×2 configuration



(b) Stage 1: Torque peak generation



(c) Stage 2: Separation

Figure 1. A group of four aerial modules in a square shape performing an undocking action. The undocking has to be a rapid action and requires the coordination of both sub-groups. The robots are connected using a passive mechanism that disconnects by generating a torque peak and performing a separation maneuver.

Another important ability of the modular systems is changing their shape depending on the task or the environment [10]. In the robotics literature, there are aerial modular systems that can be manually assembled [9], [11], [12], [13], [14], [15], self-assembly on the ground [8], self-assembly on the water [16], or even self-assemble in midair [1]. However, none of these systems is able to self-reconfigure in midair. The primary challenge is to develop a lightweight mechanism that allows modules to dock and undock during flight. Active mechanisms, e.g. electromagnets or electro-permanent magnets, offer an easy way to attach and detach [17], [18], but the electronics and additional moving parts increase the weight of the aerial vehicle affecting the flight duration and stability. In [8], a

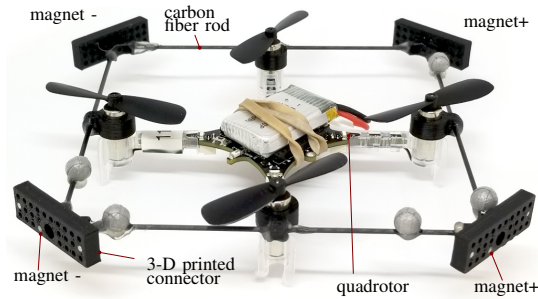


Figure 2. Module: The design is based on a quadrotor with a light-weight square frame and four 3-D printed magnet connectors.

modular aerial structure, based on a single propeller per module, was presented. The authors described the possibility to undock in midair, but the modular system was not able to fully disassemble or reach line configurations since each module was not capable of flight on its own. Additionally, no experimental evidence was provided to prove the undocking concept.

The main contribution of this paper is threefold: *i)* We design an aerial module with a lightweight passive mechanism for docking and undocking in midair. *ii)* We propose an undocking method for rectangular structures (illustrated in Figure 1). *iii)* We develop an algorithm to disassemble structures into individual modules. We discuss how our self-disassembly algorithm can be used for aerial self-reconfiguration by using self-assembly methods from the literature.

II. MODULE DESIGN

The module is a light-weight vehicle capable of flying, docking, and undocking in midair. Our previous design [1] had the ability to dock in midair, but the module-to-module connection was very strong and once the modules were connected, they were not able to self-disassemble. We extended our previous design to include the undocking capability based on an array of permanent magnets. Our new module design is shown in Figure 2.

a) Propulsion: The module is propelled by the Crazyflie 2.0 quadrotor. This platform is open-source, open-hardware and compatible with the Robot Operating System (ROS). The vehicle weighs 27 g and its maximum payload is 15 g.

b) Modular frame: The module has a square frame based on carbon fiber and 3D-printed ABS parts. The edges of the square are carbon fiber rods with a diameter of 1.37 mm, and the vertices are 3D-printed connectors. The frame is attached to the quadrotor using four 3D-printed motor mounts. The magnetic matrix lies on roll and pitch axes and allows docking of four modules on the North, South, East, and West sides. In comparison to the original version, we reduced the weight of the frame from 8.5 g to 6.7 g with final dimensions of 157 mm \times 157 mm. The total weight of our module including the modular frame is 36.7 g.

c) Docking and undocking mechanism: Active mechanisms are a very convenient and straightforward way to control module attachments. However, they require additional electronics

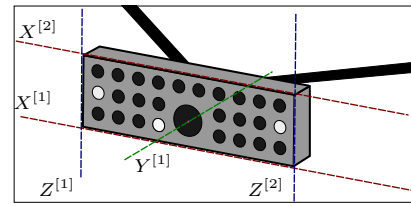


Figure 3. A connector for docking and undocking based on a magnetic matrix.

and mechanical parts that increase the payload. Due to the limited payload of micro-aerial vehicles, we designed a passive mechanism for docking and undocking in midair using an array of permanent magnets. Using a 3-D printed magnetic matrix (shown in Figure 3), different magnetic configurations can be tested to effectively determine a configuration that is compatible with the vehicle capabilities.

The dimensions of the connector are 29.17 mm \times 9.55 mm and it weighs 0.9 g. It has a matrix of 3 \times 10 holes where Neodymium Iron Boron (NdFeB) magnets can be placed. The magnets have 1.6 mm diameter and 0.8 mm thickness. The concept of using an array of small magnets as a passive mechanism for attaching and detaching was initially proposed in [19] for wall climbing.

A pair of connectors can be separated by applying forces and/or torques. There are five possible axes of rotation using torques (see Figure 3). Rotation about the roll axis $Y^{[1]}$ is an optimal way to separate a pair of modules since the shear force of the magnets is only 30% of the pull force. However, this method fails to scale when there are more than four modules in a square configuration due to incompatibility with multiple rotation axes. The $Z^{[1]}$ and $Z^{[2]}$ rotation axes are parallel to the yaw axis of the quadrotor, but in the yaw axis, the control authority of a quadrotor is a magnitude lower than the pitch and roll axes. Therefore, having one or more magnets far from $Z^{[1]}$ and $Z^{[2]}$ generates a high torque that cannot be overcome by the quadrotor. Our design uses the mechanical lever advantage through a torque to separate the magnets and to reduce the pull force for an undesired separation. We placed the magnets close to $X^{[1]}$ to rotate around this axis by generating a torque in the roll axis of the quadrotor. Since rotating around $X^{[2]}$ can generate collisions, we avoid rotations by placing the magnets far from this axis. In terms of translations, translating through the $Y^{[1]}$ and $X^{[1]}$ axis is difficult because the quadrotor does not generate any force in those axes. It would be possible to translate in the $Z^{[1]}$ axis moving one module up and one module down, but this maneuver generates a torque on the aerial structure that tilts the modules instead of translating them. This leads to the final configuration of the magnets illustrated in Figure 3.

As a summary of the connector design, we place the magnets in the matrix to avoid undesired rotations in the axis $X^{[2]}$, $Y^{[1]}$, $Z^{[1]}$, and $Z^{[2]}$, and to allow rotations in $X^{[1]}$. In this manner, the modules can fly in a cooperative way without unexpected undockings, but they can also apply a coordinated undocking maneuver. The connection is sufficiently weak to allow a pair of robots to detach when opposite maximum

torques are generated, but also sufficiently strong to avoid undesired detaching during flight. In the following section, we describe how the design for undocking a single module from a structure can be used to undock a line of modules from a rectangular structure.

III. MODEL

The basic unit of the system is the module, and it is defined as follows.

Definition 1 (Module). *A module is a flying robot that can move by itself in a three-dimensional environment and horizontally dock and undock from other modules.*

This module is based on a quadrotor platform with a square-shaped frame. The module has a mass m and the dimensions of the square frame are $w \times w$. Each module i has four vertical rotors in a square configuration, indexed by $j = 1, \dots, 4$, each with an angular speed ω_{ij} that generates vertical forces and moments

$$f_{ij} = k_F \omega_{ij}^2, \quad M_{ij} = \pm k_M \omega_{ij}^2,$$

where k_F and k_M are motor constants that can be obtained experimentally. We used $k_F = 2.04 \times 10^{-12}$ and $k_M = 2.7 \times 10^{-10}$ in our experimental setup. The sign of the moment depends on the direction of the motor spin i.e. positive for counterclockwise and negative for clockwise.

Consider a set of n connected modules. All modules are homogeneous, including shape, mass, inertia, and actuators. We define a set of connected modules as a structure.

Definition 2 (Structure). *A flying structure, S , is a non-empty set of rigidly connected modular robots that behaves as a single rigid body. These modules are horizontally connected by docking along the sides forming a planar structure.*

A. Coordinate frames

We define three main coordinate frames (illustrated in Figure 4).

1) *World coordinate frame (W):* or inertial frame is fixed and has its z -axis pointing upwards. We denote the location of the center of mass of the i th module in the world frame W by $\mathbf{x}_i \in \mathbb{R}^3$. The module attitude is represented by the Euler angles $\Theta_i = [\phi_i, \theta_i, \psi_i]^\top$ for roll ϕ_i , pitch θ_i , and yaw ψ_i .

2) *Module coordinate frame (R_i):* is defined for each robot. The origin is attached to the center of mass, the z -axis pointing upwards, and the x -axis is aligned to the front of the module. The angular velocities in the module frame are denoted by $\Omega_i = [p_i, q_i, r_i]^\top$.

3) *Structure coordinate frame (S):* is defined for a set of attached modules \mathcal{S} . The origin is attached to the center of mass of the structure. In [20] it is shown that modules can be docked in different orientations. Each module can obtain the orientation of the structure by rotating itself in the z -axis an angle of $\{0, 90, 180, 270\}$ degrees that depends on the docking face. For simplicity and without loss of generality, we assume that all modules are on the same plane and pointing to the same direction. So the Euler angles and the angular velocities

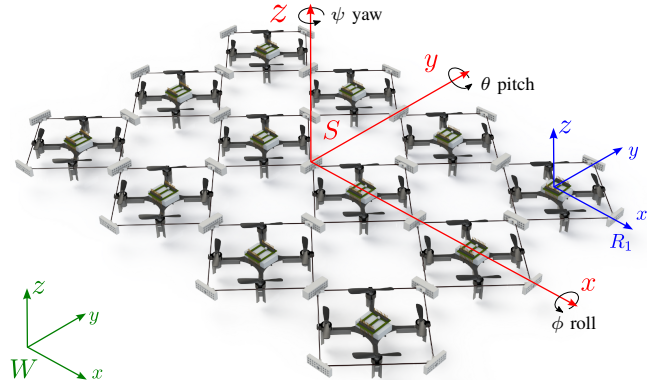


Figure 4. Coordinate frames of a structure. The world, structure, and module axes are represented by the green, red, and blue axes respectively.

of the structure are the same as all modules, i.e., $\Theta = \Theta_i$ and $\Omega = \Omega_i$, for all $i \in \mathcal{S}$.

B. Dynamics of the structure

The thrust and attitude of the structure depend on the forces and moments produced by each rotor. The total thrust F and total moments $\mathbf{M} = [M_x, M_y, M_z]^\top$ are computed as the result of all the rotor forces in the structure

$$\begin{bmatrix} F \\ M_x \\ M_y \\ M_z \end{bmatrix} = \sum_i \begin{bmatrix} 1 & 1 & 1 & 1 \\ y_{i1} & y_{i2} & y_{i3} & y_{i4} \\ -x_{i1} & -x_{i2} & -x_{i3} & -x_{i4} \\ \frac{k_M}{k_F} & -\frac{k_M}{k_F} & \frac{k_M}{k_F} & -\frac{k_M}{k_F} \end{bmatrix} \begin{bmatrix} f_{i1} \\ f_{i2} \\ f_{i3} \\ f_{i4} \end{bmatrix} \quad (1)$$

where (x_{ij}, y_{ij}, z_{ij}) denotes the location of the rotor $j = 1, \dots, 4$ that belongs to the i th module in the structure coordinate frame S . We can either control the force of each individual actuator

$$[f_{i1}, f_{i2}, f_{i3}, f_{i4}]^\top = \mathbf{u}_i, \quad (2)$$

or the desired attitude of the structure

$$[F, \phi, \theta, \psi]^\top = \mathbf{w}_S. \quad (3)$$

The last uses the attitude controller that is presented in [1]. The resultant force and moments generate translational and rotational accelerations,

$$nm \ddot{\mathbf{x}}_S = \begin{bmatrix} 0 \\ 0 \\ -nm g \end{bmatrix} + \mathbf{R}_S^W \begin{bmatrix} 0 \\ 0 \\ \sum_{ij} f_{ij} \end{bmatrix},$$

where g is the gravity constant, $\mathbf{R}_S^W \in \mathbb{R}^{3 \times 3}$ is the rotation matrix that transforms from the structure coordinate frame S to the world coordinate frame W .

Assuming that each module is symmetric and its inertia tensor is a diagonal matrix, $\mathbf{I} = \text{Diag}(I_x, I_y, I_z)$, the rotational accelerations are

$$\mathbf{I}_S \dot{\Omega} = \mathbf{M} - \Omega \times \mathbf{I}_S \Omega, \quad (4)$$

where the mass moment of inertia of the structure is

$$\mathbf{I}_S = n\mathbf{I} + m \begin{bmatrix} \sum_i y_i^2 & 0 & 0 \\ 0 & \sum_i x_i^2 & 0 \\ 0 & 0 & \sum_i x_i^2 + y_i^2 \end{bmatrix}, \quad (5)$$

where (x_i, y_i, z_i) denotes the location of the i th module in the structure coordinate frame S .

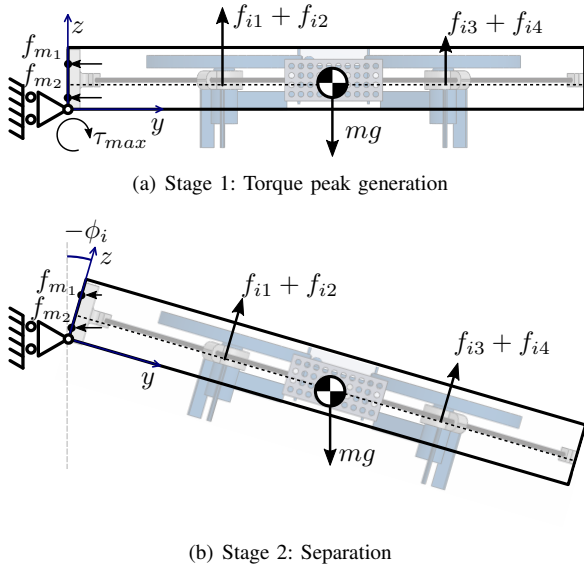


Figure 5. A single module performing the two stages to undock from a flying structure.

IV. UNDOCKING METHOD

Given a rectangular structure \mathcal{S} with $n > 1$ modules, we want to apply a maneuver to undock a substructure \mathcal{S}_1 from a substructure \mathcal{S}_2 , such that $\mathcal{S} = \mathcal{S}_1 \cup \mathcal{S}_2$. We illustrate a module connected to a structure in Figure 5(a). The module is connected to the structure through two magnetic forces, upper f_{m_1} and lower f_{m_2} . The attaching mechanism is based on two rows of magnets as it can be seen in Figure 3. Our proposed method consists of two stages to break each of the magnetic connections. Snapshots of the undocking process are presented in Figure 1. In our model, the upper f_{m_1} and lower f_{m_2} forces can be different. A high f_{m_1} requires a higher peak for Stage 1, and a high f_{m_2} requires a higher horizontal force for Stage 2. In this section, we refer to the necessary moment for undocking as torque.

A. Stage 1: Torque peak generation

In this initial stage, the module generates a sufficient torque to break the upper connection held by force f_{m_1} (see Figure 1(b)). For simplicity in this section, we place the coordinate system on the rotation point where the rotation axis matches the x -axis, the y - and z -axis match the bottom and the vertical side of the module respectively (see Figure 5(a)). Using the parallel axis theorem, we can compute the inertia tensor with respect to the new rotation axis $\hat{I}_x = I_x + mw^2/4$. Initially we study how a substructure \mathcal{S}_1 with a single module, $|\mathcal{S}_1| = 1$, can generate a torque peak. Then how the substructure \mathcal{S}_2 , $|\mathcal{S}_2| \geq 1$ generates an opposite torque. Finally a generalization for $|\mathcal{S}_1| \geq 1$, where all robots are arranged in a line that is parallel to the rotation axis.

1) *Maximum torque by a single module:* Consider a scenario where module i is undocking from a line structure. The total torque that the magnets generate is

$$\tau_m = z_{m_1} f_{m_1} + z_{m_2} f_{m_2}, \quad (6)$$

where z_{m_1} and z_{m_2} are the distances from the rotation point to the magnetic forces f_{m_1} and f_{m_2} respectively. The torque that the motor forces and the gravity generate is

$$\tau_i = y_{i1}(f_{i1} + f_{i2}) + y_{i2}(f_{i3} + f_{i4}) - y_i mg, \quad (7)$$

where y_i is the y -coordinate of the center of mass. In the single module case $y_{i1} = w/2 - d$, $y_{i2} = w/2 + d$, and $y_i = w/2$, where d is the distance from the center of mass to the rotor in the y -axis. We obtain

$$\tau_i = \frac{w}{2}(f_{i1} + f_{i2} + f_{i3} + f_{i4} - mg) - d(f_{i1} + f_{i2} - f_{i3} - f_{i4}).$$

Let f_{max} be the highest force that can be generated before motor saturation. It is straightforward to show that the maximum moment in clockwise direction, τ_{max} , that the module can generate while satisfying $\sum_j f_{ij} = mg$ is making $f_{i1} = f_{i2} = f_{max}$ and $f_{i3} = f_{i4} = f_{min}$, where $f_{min} = mg/2 - f_{max}$. Substituting in τ_i , the maximum torque that the module can generate is

$$\tau_{max} = 2d(f_{min} - f_{max}). \quad (8)$$

Hence, the control input for the torque peak is

$$\mathbf{u}_i = [f_{max}, f_{max}, f_{min}, f_{min}]^T. \quad (9)$$

Since τ_{max} is related to the physical limitation of the actuators, the magnetic forces f_{m_1} and f_{m_2} have to be designed to satisfy

$$|\tau_{max}| > |\tau_m|. \quad (10)$$

Assuming that the z_{m_2} is close to zero, the torque τ_m is mainly generated by f_{m_1} . Therefore, we can compute an upper-bound for f_{m_1} ,

$$|f_{m_1}| < \left| \frac{\tau_{max} - z_{m_2} f_{m_2}}{z_{m_1}} \right| \approx \frac{|\tau_{max}|}{z_{m_1}}. \quad (11)$$

Applying τ_{max} , and assuming that the module only rotates around the x -axis, we can compute the angular acceleration during the undocking

$$\ddot{\phi} = \frac{\tau_{max} - \tau_m}{\hat{I}_x}. \quad (12)$$

Assuming point magnets, the magnetic force f_{m_1} is reduced with the inverse of the square separation distance, which is given by

$$s = 2z_1 \sin \phi. \quad (13)$$

Based on (10), the angle $|\phi|$ increases, as well as the separation distance s , driving the magnetic force f_{m_1} to zero. With double integration of the angular acceleration $\ddot{\phi}$ starting at t_0 , we can either analytically or experimentally obtain a time t_1 that drives to modules to a desired angle ϕ^* . The angle ϕ^* only needs to be large enough to keep f_{m_1} close to zero.

In the case of bigger robots, a higher torque can be generated and consequently, the magnets can be positioned higher in the z -axis leading to a larger z_1 distance. The magnetic force is reduced with the inverse of the square separation distance, s^{-2} , and the distance z_1 grows linearly with the size of the module. Therefore, based on (13), and growing the magnetic force linearly with the size of the module, the necessary angle $|\phi|$ to break the connection is smaller as the size of the module grows. In addition, the higher inertia in (12) leads to a less aggressive angular acceleration as well.

2) *Torque by the structure*: The objective of \mathcal{S}_2 is to generate a contrary torque $-\tau_{max}$. Using (7),

$$\sum_{i \in \mathcal{S}_2} \tau_i = -\tau_{max}. \quad (14)$$

Additionally, the modules in \mathcal{S}_2 have to compensate gravity to maintain altitude

$$\sum_{k \in \mathcal{S}_2} \sum_{j \in \{1, \dots, 4\}} f_{kj} = mg|\mathcal{S}_2|. \quad (15)$$

The dynamical system of the structure \mathcal{S}_2 is redundant. We need to satisfy (14) and (15) using $4|\mathcal{S}_2|$ actuators. In [21], [8], the authors showed that minimizing the sum of the squares of the forces also minimizes the shear forces,

$$\Phi = \min \sum_{i \in \mathcal{S}_2} \sum_{j \in \{1, \dots, 4\}} f_{ij}^2,$$

subject to (15), (14) and

$$0 \leq f_{ij} \leq f_{max}.$$

Therefore, the input forces f_{ij} are obtained by using a quadratic programming solver for Φ .

3) *Undocking more than one module*: We can extend the single-module peak generation to undock either border rows or border columns from a rectangular structure. Undocking more than one module is possible, $|\mathcal{S}_1| > 1$, using the same peak generation if the modules are in a line that is parallel to the rotation axis. Hence, in a structure with a rectangular shape, we can undock the leftmost and the rightmost columns, as well as the upmost and downmost rows.

Lets assume that the sub-structure \mathcal{S}_1 on the border row (or column) has l_1 modules, and \mathcal{S}_2 has l_2 modules. All modules in \mathcal{S}_1 are aligned with the rotation axis. Hence, the inertia in the y - and z -axes grows fast based on (5), but the inertia in the x -axis is proportional to the number of modules, i.e., $\hat{I}_x(l_1) = l_1 \hat{I}_x$. The torque that the l_1 modules generate is $\tau_{max}(l_1) = l_1 \tau_{max}$ and that is the same for the l_1 connectors $\tau_m(l_1) = l_1 \tau$. Therefore, similar to (12), the sub-structure \mathcal{S}_1 maintains the same angular acceleration of a single module

$$\ddot{\phi}(l_1) = \frac{\tau_{max}(l_1) - \tau_m(l_1)}{\hat{I}_x(l_1)} = \frac{\tau_{max} - \tau_m}{\hat{I}_x}. \quad (16)$$

In this way, the modules on the border row (or column) apply the same control input from (9), and the sub-structure \mathcal{S}_2 applies the same solution for Φ .

B. Stage 2: Separation

After Stage 1, the substructure \mathcal{S}_1 generates a sufficient angle to drive the magnetic force f_{m_1} to zero. However, the aperture angle does not significantly affect f_{m_2} as it is close to the rotation axis. We illustrate the final state of Stage 1, and the beginning of Stage 2 in Figure 5(b). The objective of Stage 2 is to break the second attaching point by generating a horizontal force (see Figure 1(c)).

For the sub-structure \mathcal{S}_1 , lets assume that there exist a thrust F_1 and an angle ϕ_1^* that maintains f_{m_1} close to zero and satisfies

$$F_1 \sin|\phi_1^*| > l_1 |f_{m_2}|, \text{ and} \quad (17)$$

$$F_1 \cos \phi_1^* = l_1 mg. \quad (18)$$

Solving these two equations, we obtain a lower-bound

$$\phi_1^* > \arctan\left(\frac{|f_{m_2}|}{mg}\right), \quad (19)$$

and the thrust is just a function of the desired angle $F_1 = l_1 mg / \cos \phi_1^*$. Using the attitude input from (3), we can generate the control input

$$\mathbf{w}_{\mathcal{S}_1} = [F_1, -\phi_1^*, 0, 0]^\top. \quad (20)$$

For the sub-structure \mathcal{S}_2 , we have a similar procedure to break l_1 links, $F_2 \sin|\phi_2^*| > l_1 |f_{m_2}|$, and $F_2 \cos \phi_2^* = l_2 mg$. Then the lower-bound is

$$\phi_2^* > \arctan\left(\frac{l_1 |f_{m_2}|}{l_2 mg}\right). \quad (21)$$

Since $l_2 \geq l_1$ in a rectangular structure, the lower-bound of ϕ_2^* is equal or lower than ϕ_1^* . Then we can do $\phi_2^* = -|\phi_1^*|$, and the attitude control input is

$$\mathbf{w}_{\mathcal{S}_2} = [F_2, \phi_1^*, 0, 0]^\top. \quad (22)$$

The inputs from (20) and (22) are similar to the input of a position controller sending robots in perpendicular directions of the rotation axis. In the position controller, F_1 and F_2 are the necessary thrust to hover while compensating the gravity, and the angles ϕ_1^* and ϕ_2^* are the tilting angles to generate acceleration in opposite directions for translation. Therefore, a position controller can be used as an alternative for Stage 2. Without loss of generality, we assume that y -axes of the structures are aligned to the y -axis of the global frame. We can show that the modules perform the separation task by checking the accelerations,

$$\ddot{y}_{\mathcal{S}_1} = \frac{F_1 \sin(\phi_1^*) - l_1 f_{m_2}}{l_1 m}, \text{ and } \ddot{y}_{\mathcal{S}_2} = -\frac{F_2 \sin(\phi_1^*) - l_1 f_{m_2}}{l_2 m}$$

Since \mathcal{S}_1 translates in the positive direction to the y -axis and the \mathcal{S}_2 translates in the contrary direction, we can conclude that the separation process is completed.

V. SELF-DISSASSEMBLY ALGORITHM

We propose a recursive algorithm that receives a rectangular structure as an input and the output is a set of individual modules in a grid formation. The self-disassembly sequence is summarized in Algorithm 1. The stop condition of the recursion is in lines 1 and 2, where the output is a structure with a single module. We disassemble the structure by undocking rows and columns. If the rectangular structure has more columns than rows (line 8), we proceed to undock the upmost row. The undocking action is performed in line 4. Then we move each of the substructures in opposite directions toward the y -axis. The final separation distance between the two structures is 3ℓ . We recall that a position controller generates a similar input as the one in Stage 2 in (20). Therefore, Stage 2

Algorithm 1: Self-dissassembly(\mathcal{S})

```

1 if  $|\mathcal{S}| = 1$  then
2   return  $\mathcal{S}$                                      ▷ Single module
3 if  $rows(\mathcal{S}) > columns(\mathcal{S})$  then
4    $\mathcal{S}_u, \mathcal{S}_b = \text{undockUpmostRow}(\mathcal{S})$ 
5   RelativeTranslation( $\mathcal{S}_u, [0, -\ell, 0]$ )
6   RelativeTranslation( $\mathcal{S}_b, [0, 2\ell, 0]$ )
7   Self-dissassembly( $\mathcal{S}_u$ )
8   Self-dissassembly( $\mathcal{S}_b$ )
9 else
10   $\mathcal{S}_l, \mathcal{S}_r = \text{undockLeftmostRow}(\mathcal{S})$ 
11  RelativeTranslation( $\mathcal{S}_l, [-\ell, 0, 0]$ )
12  RelativeTranslation( $\mathcal{S}_r, [2\ell, 0, 0]$ )
13  Self-dissassembly( $\mathcal{S}_l$ )
14  Self-dissassembly( $\mathcal{S}_r$ )

```

and the translation can be integrated into the same control command. Finally, we recursively call the self-disassembly algorithm for each of the sub-structures. In the case where the structure has more rows than columns, we apply a similar procedure from line 10 to 14, but undocking the leftmost row. We highlight that calling the self-disassembly functions in lines 7,8,13 and 14 are sub-process that are independent, and executed in parallel. The relative translation (lines 4,5,11 and 12) will guarantee to avoid collisions during the parallel disassembling.

a) Time complexity: Assuming that each undocking action is performed in a time unit. Given a rectangular structure of $M \times N$ modules, the algorithm performs iterative undocking actions for rows and columns. It is similar to undocking all the columns, one by one, and then undocking individual modules from each column. The algorithm performs $N - 1$ undocking steps for columns and $M - 1$ undocking steps for rows. Hence the time complexity of the algorithm is $\mathcal{O}(N + M)$.

The best case for the algorithm is a square shape $n = N \times N$. It performs in $\mathcal{O}(\sqrt{n})$. The worst case is the line shape $n = 1 \times N$, because it does not parallelize undocking actions. Each module in the structure has to be undocked one by one; performing the disassembly task in $\mathcal{O}(n)$.

b) Self-reconfiguration: In this paper, we specifically focus on the self-disassembly process, but this algorithm can be used to perform aerial self-reconfiguration. In a previous work [22], we proposed a fast self-assembly algorithm for ground modules, but it can be applied to aerial modules as well. The main advantage of this algorithm is parallelizing docking actions. Starting with independent modules, pairs of modules get docked, then pairs and pairs are docked, and so on. Hence for rectangular structures, the time complexity is $\mathcal{O}(\log n)$.

A structure can reconfigure its rectangular shape $M_1 \times N_1$ to another rectangular shape $M_2 \times N_2$. To achieve this, we use Algorithm 1 to disassemble all the modules, and then the self-assembly algorithm in [22]. Since the bottleneck is in the disassembly process, the time complexity of the self-reconfiguration is $\mathcal{O}(N_1 + M_1)$.

VI. EXPERIMENTS

In our experimental testbed, we used six Crazyflie robots and the modular frame that is described in Section II. The robot pose is obtained using a motion capture system (VICON) operating at 100 hz. The angular velocities for the attitude controller are based on the internal IMU sensors. We use a central computer for position control and high-level commands. Attitude control commands are sent to the robots at 60 hz via the Crazyradio PA 2.4 GHz radio USB dongle. Our framework was implemented using Python and ROS. Our nodes are integrated with the Crazyflie-ROS node [23] to control the robots. The torque peak generation and cooperative attitude controller was implemented directly on the Crazyflie firmware¹.

The length of the module is $w = 157$ mm, and the distance to the motor is $d = 32.5$ mm. The weight of the module is $m = 36.7$ g. The pull force of each magnet is 31.75 g according to the manufacturer specifications. The magnetic forces f_{m_1} and f_{m_2} were determined by the number of magnets per row in the magnetic matrix (see Figure 3). The equations (11) and (17) define the upper bounds for the magnetic forces depending on the module constraints. The placement of the magnets in the magnetic matrix was determined experimentally based on three factors: *i)* The peak torque should be able to separate the first row of magnets and open the joint; *ii)* applying stage 2 (without stage 1) should not be sufficient to separate the modules; and *iii)* two forces should be placed horizontally apart to avoid undocking by applying a torque in the z -axis. These factors reduce unexpected undockings during flight. Our best configuration is illustrated in Figure 3. The values of the forces are $f_{m_1} = 63.6$ gf, and $f_{m_2} = 31.75$ gf. The distances to the rotation axis are $z_{m_1} = 4.73$ mm, and $z_{m_2} = 1.94$ mm. Hence, the torque of the magnets from (6) is $\tau_m = 361.95$ gf-mm.

For the torque peak generation, we used $f_{i1} = f_{i2} = 14.04$ gf, and $f_{i3} = f_{i4} = 4.31$ gf, generating a torque $\tau_{max} = 632.45$ gf-mm. The peak is generated for 240 ms in open-loop control. The duration of the peak can be obtained analytically as we described in Section IV-A, but the calculated inertia term for the real robot is not accurate, so we opted to obtain the duration of the peak experimentally. This can be obtained using a bisection approach where the goal is to find a safe duration that reaches the desired opening angle without overshooting.

A. Undocking

We performed several experiments to show that our undocking method can be performed in different configurations. We want to show that a pair of modules can be undocked, as well as rows and columns in a rectangular structure. Our main experiments for a team of six modules are: *a)* Undocking a pair of robots; *b)* Undocking a square structure 2×2 ; *c)* Undocking a module from a line of three robots (1×3); *d)* Undocking a row of modules from a rectangular structure 2×3 ; and *e)* undocking a column of modules from a rectangular structure

¹The ModQuad firmware is available at:
<https://github.com/dsaldana/modquad-firmware>

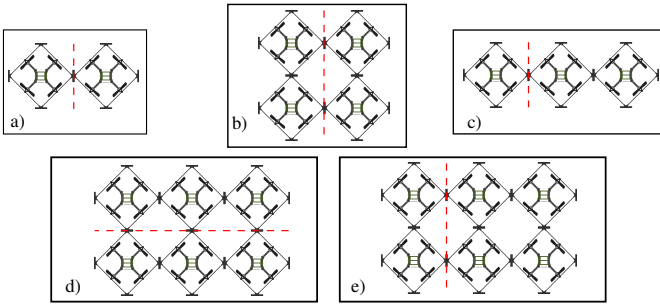


Figure 6. Undocking experiments. Each panel shows the structure that performs the undocking action. The dashed line represents the division of the two sub-structures.

2×3 . The main experiments presented in the accompanying video ² and summarized in Figure 6.

We wanted to carefully study the tilting angle ϕ during the undocking procedure. Structures with a small number of modules can quickly recover from a high angle. We observed the recovery of two modules with $\phi \approx 80^\circ$. However, large structures have slower behavior due to the high inertia [1]. Using the parameters described above, the maximum angle is between 20° and 30° . We illustrate the tilting angle ϕ in time for each of the experiments in Figure 7. In these plots, we show the data obtained from the VICON system after applying a Gaussian filter (with $\sigma_t = 2$ and $\sigma_\phi = 1$) to smooth the discrete sampling and to remove the noise. The green region represents the time interval where the undocking action starts. In this time interval, each module updates its attitude controller for undocked structures, so the sub-structures will be prepared to recover after the peak generation. The update consists on changing eight integers that are sent from the central computer to each module. These parameters abstract the position of the module in the structure and affect the way forces are distributed in the structure. More details about the attitude controller are in [1]. Since not using the proper attitude controller for the structure generates instability, the modules rapidly switch to the controller of Stage 1. The red region represents the time interval of Stage 1 where the peak generation is performed. In this stage, we switch from the attitude controller to the undocking controller in (9). We can observe that the peak significantly increases the angle between each pair of sub-structures. After the red region, the robots continue with Stage 2 which is performed by the position controller that takes each of the sub-structures 500 mm apart from the initial location. We can observe that the undocking actions were performed in less than 5 seconds for all the experiments.

Symmetrically undocking structures 7(a), 7(b), and 7(d) show equal contribution in the undocking axis. Asymmetrical structures 7(c) and 7(e) show decreased angular acceleration and subsequent difference in undocking angle ϕ . In experiments (c) and (d), we can see that the larger structures present a slower behavior since the inertia grows faster than the applied torque.

²The video of the experiments is available at: https://youtu.be/N80_sG0gjhE

B. Self-reconfiguration

We show that the undocking actions can be combined for self-disassembling. We applied Algorithm 1 to a rectangular structure of 2×3 modules. We illustrate the self-disassemble process, step by step, in Figure 8. During the first step, the six robots start together we undock the leftmost column (see Figure 8(a)). The sub-structure of four modules is translated to the right to satisfy the distance 2ℓ (see Figure 8(b)), where $\ell = 0.5$ m. The second undock is performed in Figure 8(c). And finally, three pairs of robots are undocked in parallel (see Figure 8(d)). Following our proposed algorithm, the structure was disassembled in four steps.

VII. CONCLUSIONS AND FUTURE WORK

In this work, we present a module design that uses a passive mechanism for docking and undocking. We propose a method based on two stages for inflight undocking. This method can be applied to divide rectangular structures into two sub-structures. Using a sequence of undocking actions and translations, we propose an algorithm to efficiently disassemble a structure into individual modules. Our experiments validated our proposed method for undocking and the algorithm.

For the undocking method, we proposed a rapid torque generation in open-loop control. For future work, exploring less aggressive maneuvers in a closed-loop control can improve the undocking reliability and avoid tuning the duration of the torque peak generation. In object transportation, new flight controllers need to be developed to preserve the connected structure while supporting external forces and moments.

REFERENCES

- [1] D. Saldaña, B. Gabrich, G. Li, M. Yim, and V. Kumar, "Modquad: The flying modular structure that self-assembles in midair," in *2018 IEEE International Conference on Robotics and Automation (ICRA)*, May 2018, pp. 691–698.
- [2] B. Gabrich, D. Saldaña, V. Kumar, and M. Yim, "A flying gripper based on cuboid modular robots," in *2018 IEEE International Conference on Robotics and Automation (ICRA)*, May 2018, pp. 7024–7030.
- [3] J. Seo, M. Yim, and V. Kumar, "Assembly sequence planning for constructing planar structures with rectangular modules," in *2016 IEEE International Conference on Robotics and Automation (ICRA)*, May 2016, pp. 5477–5482.
- [4] H. Nguyen, S. Park, and D. Lee, "Aerial tool operation system using quadrotors as rotating thrust generators," in *2015 IEEE/RSJ International Conference on Intelligent Robots and Systems (IROS)*, Sep. 2015, pp. 1285–1291.
- [5] D. Mellinger, M. Shomin, N. Michael, and V. Kumar, "Cooperative grasping and transport using multiple quadrotors," *Springer Tracts in Advanced Robotics*, vol. 83 STAR, pp. 545–558, 2012.
- [6] F. Augugliaro, S. Lupashin, M. Hamer, C. Male, M. Hehn, M. W. Mueller, J. S. Willmann, F. Gramazio, M. Kohler, and R. D'Andrea, "The flight assembled architecture installation: Cooperative construction with flying machines," *IEEE Control Systems*, vol. 34, no. 4, pp. 46–64, 2014.
- [7] Q. Lindsey, D. Mellinger, and V. Kumar, "Construction of Cubic Structures with Quadrotor Teams," *Mechanical Engineering*, 2011.
- [8] R. Oung and R. D'Andrea, "The distributed flight array: Design, implementation, and analysis of a modular vertical take-off and landing vehicle," *The International Journal of Robotics Research*, vol. 33, no. 3, pp. 375–400, 2014.
- [9] M. J. Duffy and T. C. Samaritano, "The lift! project—modular, electric vertical lift system with ground power tether," in *33rd AIAA Applied Aerodynamics Conference*, 2015, p. 3013.
- [10] J. Seo, J. Paik, and M. Yim, "Modular reconfigurable robotics," *Annual Review of Control, Robotics, and Autonomous Systems*, 2018.

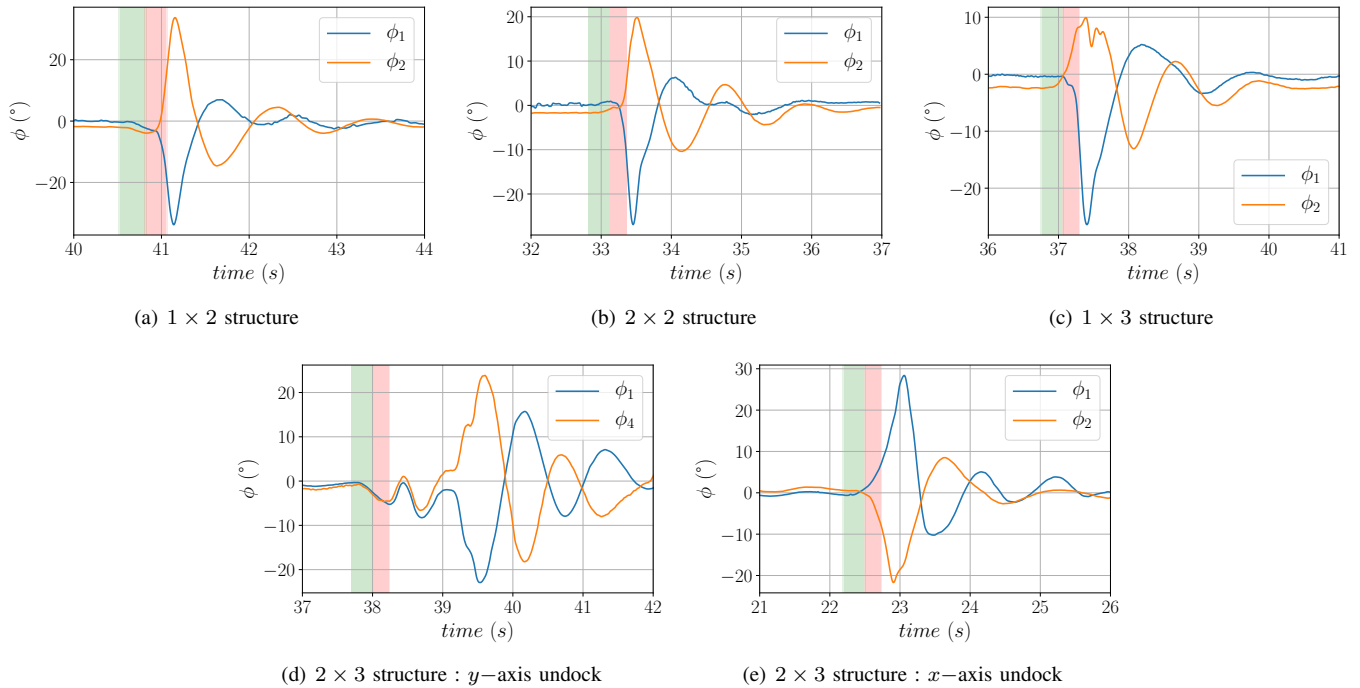


Figure 7. Undocking experiments for different structures. It shows the change tilting angle ϕ in time for each of the sub-structures during the undocking action. The green region highlights the time interval for updating the onboard attitude controller. The red region highlights the torque peak generation for Stage 1.

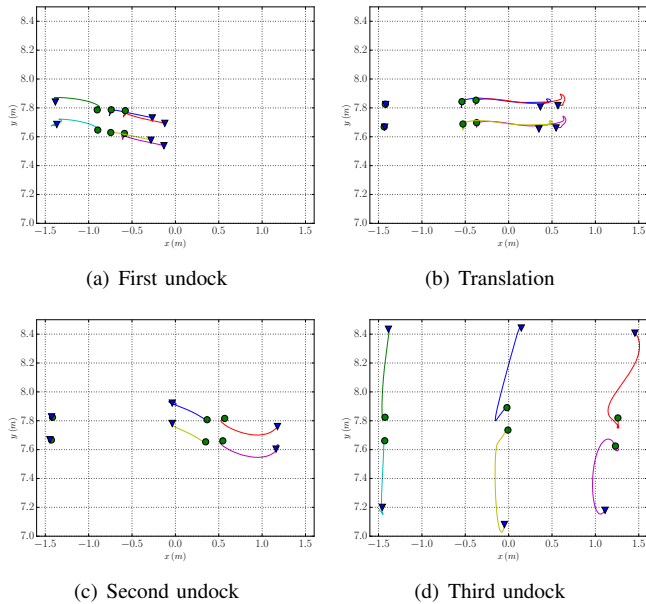


Figure 8. Trajectories for self-disassembly of a 2×3 structure. Green circles represent initial locations and blue triangles represent final locations.

[11] R. Naldi, F. Forte, and L. Marconi, "A class of modular aerial robots," in *2011 IEEE Conference on Decision and Control and European Control Conference*, Dec 2011, pp. 3584–3589.

[12] A. Torre, R. Naldi, A. Riccò, D. Mengoli, and L. Marconi, "An over-actuated modular platform for aerial inspection and manipulation," in *2013 IEEE/RSJ International Conference on Intelligent Robots and Systems*, Nov 2013, pp. 2084–2084.

[13] R. Naldi, F. Forte, A. Serrani, and L. Marconi, "Modeling and control of a class of modular aerial robots combining under actuated and fully actuated behavior," *IEEE Transactions on Control Systems Technology*,

vol. 23, no. 5, pp. 1869–1885, Sept 2015.

[14] M. Zhao, K. Kawasaki, T. Anzai, X. Chen, S. Noda, F. Shi, K. Okada, and M. Inaba, "Transformable multirotor with two-dimensional multilinks: Modeling, control, and whole-body aerial manipulation," *The International Journal of Robotics Research*, vol. 37, no. 9, pp. 1085–1112, 2018. [Online]. Available: <https://doi.org/10.1177/0278364918801639>

[15] H. Yang, S. Park, J. Lee, J. Ahn, D. Son, and D. Lee, "Lasdra: Large-size aerial skeleton system with distributed rotor actuation," in *2018 IEEE International Conference on Robotics and Automation (ICRA)*, May 2018, pp. 7017–7023.

[16] I. O'Hara, J. Paulos, J. Davey, N. Eckenstein, N. Doshi, T. Tosun, J. Greco, J. Seo, M. Turpin, V. Kumar, and M. Yim, "Self-assembly of a swarm of autonomous boats into floating structures," *Proceedings - IEEE International Conference on Robotics and Automation*, pp. 1234–1240, 2014.

[17] K. Yanagimura, K. Ohno, Y. Okada, E. Takeuchi, and S. Tadokoro, "Hovering of mav by using magnetic adhesion and winch mechanisms," in *2014 IEEE International Conference on Robotics and Automation (ICRA)*, May 2014, pp. 6250–6257.

[18] J. Thomas, M. Pope, G. Loianno, E. W. Hawkes, M. A. Estrada, H. Jiang, M. R. Cutkosky, and V. Kumar, "Aggressive Flight for Perching on Inclined Surfaces," *Journal of Mechanisms and Robotics*, vol. 8, no. October, pp. 1–10, 2015.

[19] J. Berengueres, K. Tadakuma, T. Kamoi, and R. Kratz, "Compliant distributed magnetic adhesion device for wall climbing," in *Proceedings 2007 IEEE International Conference on Robotics and Automation*, April 2007, pp. 1256–1261.

[20] G. Li, B. Gabrich, D. Saldaña, M. Yim, and V. Kumar, "Modquadvi: A vision-based self-assembling modular quadrotor," in *2019 IEEE International Conference on Robotics and Automation (ICRA)*, May 2019.

[21] O. Harkegard and S. T. Glad, "Resolving actuator redundancy—optimal control vs. control allocation," *Automatica*, vol. 41, no. 1, pp. 137–144, 2005.

[22] D. Saldaña, B. Gabrich, M. Whitzer, A. Prorok, M. F. Campos, M. Yim, and V. Kumar, "A decentralized algorithm for assembling structures with modular robots," in *2017 IEEE/RSJ International Conference on Intelligent Robots and Systems (IROS)*.

[23] W. Hönig and N. Ayanian, *Flying Multiple UAVs Using ROS*. Springer International Publishing, 2017, pp. 83–118.